Spin Hall Magnetoresistance and Spin–Orbit Torque Efficiency in Pt/FeCoB Bilayers

Spin Hall Magnetoresistance and Spin–Orbit Torque Efficiency in Pt/FeCoB Bilayers

Alessandro Magni[1], Vittorio Basso[1], Alessandro Sola[1], Gabriel Soares[1], Nicola Meggiato[1,2], Michaela Kuepferling[1], Witold Skowroński[3], Stanisław Łazarski[3], Krzysztof Grochot[3], Mehran Vafaee Khanjani[4], Juergen Langer[4], and Berthold Ocker[4]

[1]Istituto Nazionale di Ricerca Metrologica, 10135 Turin, Italy
[2]Department of Electronics and Telecommunications, Politecnico di Torino, 10129 Turin, Italy
[3]Institute of Electronics, AGH University of Science and Technology, 30059 Kraków, Poland
[4]Singulus Technologies AG, 63796 Kahl am Main, Germany

The spin Hall magnetoresistance (SMR) of Pt/FeCoB bilayers with in-plane magnetocrystalline anisotropy was analyzed with respect to a second-order effect in the sensing current, which acts, through the spin Hall effect in Pt, as a torque on the magnetization of the ferromagnetic (FM) layer and changes slightly its configuration. This leads to a small current-dependent shift of the SMR curves in field that allows, in structures with a multidomain state (e.g., Hall bars), the determination of the sign of the magnetic remanence. The SMR measurements were performed as a function of the Pt thickness and the spin Hall angle, and the diffusion length and the field-like and damping-like spin–orbit-torque (SOT) efficiency were determined. The results were compared with the values obtained from harmonic Hall voltage and SOT-FM resonance (FMR) measurements and show a good agreement.

Index Terms— **FeCoB, Pt, spin Hall effect, spin Hall magnetoresistance (SMR), spin–orbit torque.**

I. Introduction

THE current-induced spin–orbit torque (SOT) [1]–[4] is the physical phenomenon by which a magnetic moment current (or spin current), generated by a heavy metal (HM) layer, induces a magnetic torque on a side ferromagnetic (FM) layer. The magnetic torque is able to induce dynamical phenomena in the ferromagnet, including magnetization oscillations [5] and switching [6]. Such bilayers are therefore considered as promising elements to be applied as microwave generators and as magnetic bits of classical nonvolatile memories as well as of modern artificial neural networks [1].

One of the key features of the HM/FM bilayers to be used as magnetic bits in magnetic memories or sensors is the possibility to either write or read the magnetic state by electric means. Here, the possibilities depend much upon the anisotropy type realized in the FM layer. With perpendicular-to-plane magnetic anisotropy (PMA), the writing is performed by the precessional toggle switching between positive and negative saturation magnetization [7]. The reading of the magnetization state is possible by a voltage measurement through the anomalous Hall effect of the FM. While the development of magnetic memories is nowadays oriented toward the PMA [8]–[10], in-plane anisotropy is still of interest, also for applications such as sensors, since they do not require ultrathin magnetic films and are characterized by more stable and lower noise signals [11]–[13]. With in-plane anisotropy, the writing is performed either by the precessional or the damped switching, but the reading is more difficult. One possibility is to introduce a second interface made of a tunnel junction between the FM layer and another FM layer with fixed magnetization direction [14]. In this way, the reading is performed by means of the tunnel magnetoresistance (TMR) between the two ferromagnets. Such a device not only becomes rather complex from the point of view of the preparation, but it also requires to optimize SOT together with the TMR. Alternatives for reading the magnetization state and evaluating the SOT efficiency would be welcome.

Recently, Liu *et al.* [15] have suggested that the magnetization state, which is written by a current pulse, could be read by an alternating sense current pulse of lower amplitude. By the comparison of the magnetoresistance signal obtained by the two current pulses of opposite sign, the spin–orbit field and the SOT efficiency can be evaluated. In their work, the latter is obtained from magnetization switching experiments (i.e., magnetization reversal by the current in the HM) in Hall bars, an experiment that depends on the magnetization or domain configuration and dynamics in the Hall bar and on the strength of the SOT. However, a detailed analysis of the relation between magnetization state and SOT is missing.

We point out that: 1) the magnetoresistance measurements are performed in a structure (Hall bar) that is not a bistable unit, but the magnetization M is a hysteretic function of the applied field, i.e., the magnetization reversal occurs by nucleation and propagation of domain walls, and 2) the mechanism proposed in [15] is a second-order effect in the current. The spin current generated by the spin Hall effect and injected in the FM layer induces a change of the magnetization configuration by SOT, which causes a shift of the spin Hall magnetoresistance (SMR) curve as a function of magnetic field. We show here that a detailed analysis of the SMR curves

Manuscript received March 16, 2021; revised April 30, 2021; accepted May 19, 2021. Date of publication May 28, 2021; date of current version January 20, 2022. Corresponding author: M. Kuepferling (e-mail: m.kuepferling@inrim.it).

Color versions of one or more figures in this article are available at https://doi.org/10.1109/TMAG.2021.3084866.

Digital Object Identifier 10.1109/TMAG.2021.3084866

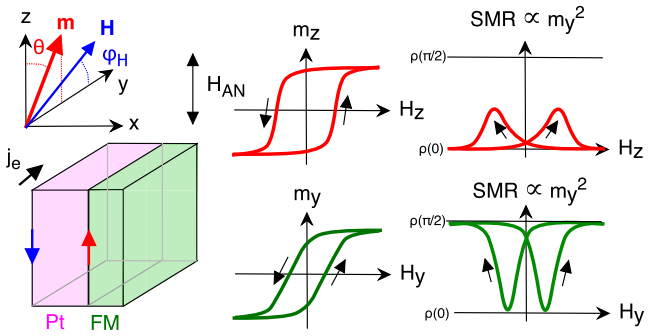

Fig. 1. Left: scheme of the heterostructure composed of a spin Hall metal (usually a HM; here Pt) and an FM metal (here $Fe_{60}Co_{20}B_{20}$). The electric current, along y, generates in the metal a current of magnetic moments along z flowing along x: $j_{x,M_z} = \theta_{SH}(\mu_B/e)j_{e,y}$ where θ_{SH} is the spin Hall angle (positive for Pt and negative for W and Ta). The FM has a magnetic anisotropy along z. Right: illustration of the relation between the magnetization curves and the SMR signal for both a magnetic field applied along z (red curves) and y (green curves).

as a function of field and electric current shows the influence of SOT on the magnetization state. This analysis may help to read the remanence state and to investigate the performance of SOT even if the spin current generated by the spin Hall effect is not large enough to reverse the magnetization direction in an extended structure, such as a Hall bar.

II. Experiment

In this article, we performed an experimental investigation of the SMR [16] in Pt/FeCoB bilayers, in order to shed a clearer light upon the mechanism envisaged by Liu *et al.* [15]. We compared the results with the harmonic Hall voltage analysis and SOT-induced FM resonance (FMR) performed in the same heterostructures in order to validate the approach.

The samples are HM/FM heterostructures with HM = Pt (wedge 4–19 nm) and FM = $Fe_{60}Co_{20}B_{20}$ (2 nm) deposited by Singulus Technologies AG using magnetron sputtering. All samples were annealed for 2 h at 310 °C in a magnetic field of 1 T in order to develop an in-plane magnetic anisotropy along the z-axis (see Fig. 1). For all measurements, the films were patterned into μm-size Hall bars/crosses (SMR-bar: length 70 μm along y and width 6 μm along z; SOT-FMR-cross: length 20 μm along z and width 30 μm along y; harmonic Hall-cross: length 30 μm along z and width 10 μm along y) using optical lithography and ion-beam etching with Ti/Au contact pads.

Magnetooptic Kerr effect measurements (MOKE) were performed by recording the magnetic contrast of the Hall bar as a function of the applied magnetic field. This contrast is related to the normalized component of the magnetization in the plane of incidence [17], and we defined the technical value of M_S as the recorded light intensity value at the maximum applied field $\mu_0 H = 10$ mT. The setup includes a Hamamatsu C9100 camera equipped with a 50× objective (N.A. = 0.55). For the application of the magnetic field along the y- and z-directions, we employed a calibrated four-pole electromagnet.

SMR measurements were performed following the protocol mentioned in [15]. For the four-point resistance measurement, a Keithley 6221 source was used, which provides 60 ms current pulses triggered together with a Keithley 2182A nanovoltmeter for the voltage acquisition. The magnetic field was calibrated by means of a Hall probe in a four-pole electromagnet, both in the y- and z-directions.

SOT-FMR measurements were performed by injecting an amplitude-modulated radio frequency (RF) current of a power of 16 dBm with frequencies between 4 and 12 GHz to the Hall-cross structure. The mixing voltage was measured by a lock-in amplifier synchronized to the RF signal.

The harmonic Hall measurement was performed at a low-frequency signal of 284 Hz and 1 V. The first- and second-harmonic signals were detected via a lock-in amplifier, dependent on the in-plane angle φ_H between the current and the magnetic field.

III. Results and Discussion

The SMR signal is the change of the electric resistivity of the HM with the angle of the magnetization of the FM layer with respect to a fixed electric current direction, induced by the spin Hall effect. The SMR theory [4], [18], [19] provides the equation

$$\frac{\varrho(\theta) - \varrho(0)}{\varrho(0)} = \Delta\hat{\varrho}_{SMR} \sin^2\theta \tag{1}$$

where $\Delta\hat{\varrho}_{SMR}$ is a coefficient to be determined. When this equation is applied to a multidomain magnetic state, one can write

$$\frac{\varrho(\theta) - \varrho(0)}{\varrho(0)} = \Delta\hat{\varrho}_{SMR} m_y^2. \tag{2}$$

Therefore, the SMR provides a method to evaluate the component of the magnetization along y and m_y^2. The sketch in Fig. 1 shows the hysteresis loops with magnetic field along z and y and the corresponding components of m_y^2 for the two processes. The inversion of the magnetization along z corresponds to the acquisition of a small component along y at the coercive field. This is due to the fact that the magnetization process involves the rotation of magnetic domains and the motion of domain walls that give an overall contribution to the magnetization along y even if the driving field is along z. Fig. 2 shows the comparison between MOKE loops with magnetic field along z and along y. The loop shape along the z-axis is more rectangular and indicates the magnetic easy anisotropy axis. With the field along y, the hysteresis loop is still present, but it has lower coercivity and it indicates that the magnetization process is perpendicular to the anisotropy direction. If the SMR is measured along the two magnetization processes, one obtains the plots of Fig. 2 (bottom). It is clearly visible that, while the process along y is able to span the full range of the SMR, the resistivity for the process along z increases only in correspondence of the coercive fields.

The SMR is a straightforward method when the FM layer is an insulator [20], while with a metallic FM, in which the testing electric current is not confined in the HM layer only, it is accompanied by additional effects, such as the anisotropic magnetoresistance (AMR) of the FM. However, in our case, the ratio of the FM/HM resistivities is a factor of 10. The contribution to the FM layer to the total resistance

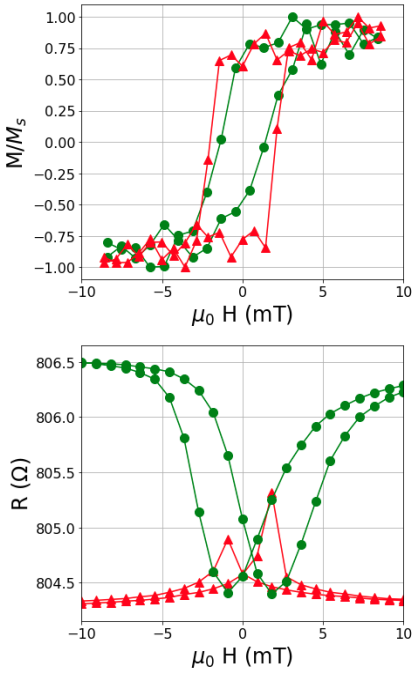

Fig. 2. Comparison between the MOKE loop (top panel) and the SMR signal (bottom panel). The MOKE loop along the z-axis (red triangles) is more rectangular and indicates the magnetic easy anisotropy axis with respect to the loop along the y hard axis (green circles). The SMR signal generated by an electrical current $I = 1$ mA is much more pronounced with the field along the y-axis (green circles) where the current is parallel to the field, while it shows a small peak close to the coercivity when the field is along the z-axis (red). Sample Pt thickness $d_{Pt} = 6.1$ nm and current density $j_e = 2.5 \cdot 10^{10}$ Am^{-2}.

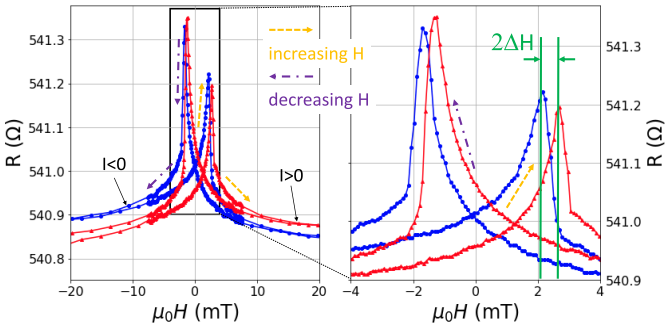

Fig. 3. SMR loops with ($I = \pm$ 10 mA, Pt thickness 7.6 nm) and zoom (right panel) showing the horizontal displacement ΔH with respect to positive (red curve) and negative (blue curve) current. The resistance reading discriminates the magnetic states at remanence.

is around 3% and the AMR of FeCoB is around 0.1%, while the SMR of Pt is around 1%. Therefore, the contribution of AMR is safely negligible.

The presence of a nonperfectly squared loop along z can be an advantage because it offers the possibility to detect the magnetization state by means of the SMR even in a configuration in which it would be precluded for a perfect bistable switching. The idea is that the electric current used to sense the SMR necessarily acts as a small torque on the FM magnetization, and therefore, it slightly alters the original magnetic state, causing a shift of the SMR curves (see Fig. 3). However, the effect of the torque depends on both the sign of

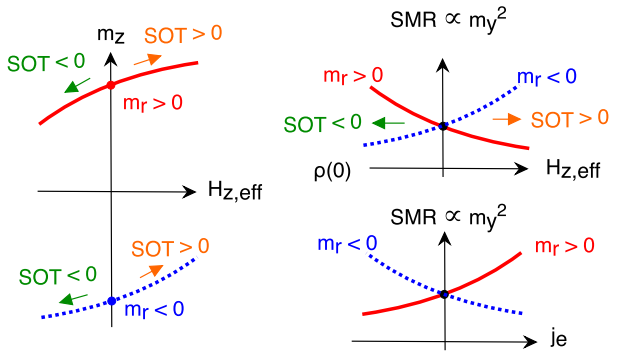

Fig. 4. Scheme illustrates the relationship between remanence state and SMR signal. The electric current density j_e acts through the spin Hall effect as a torque on the magnetization and shifts the magnetization curves.

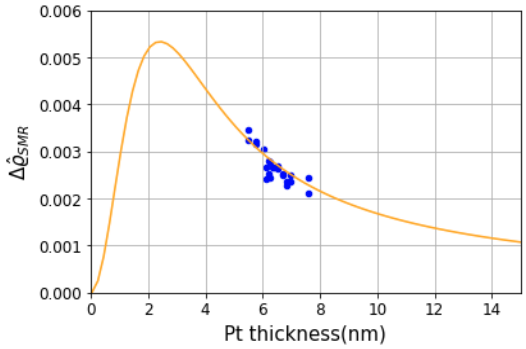

Fig. 5. $\Delta\hat{\varrho}_{\mathrm{SMR}}$ as a function of Pt thickness. Blue points: measured data. Yellow curve: fit following (3) using $G_c = 1 \cdot 10^{16}\,\Omega^{-1}\mathrm{m}^{-2}$, $\theta_{\mathrm{SH}} = 0.14$, and $l_{Pt} = 1.1$ nm.

the current and the sign of the remanence. Considering the torque introduced by the spin Hall effect of Pt (which has a positive spin Hall angle θ_{SH} [20]), its effect is explained in the scheme of Fig. 4. On the left side of the figure, it is shown that positive and negative SOT change the remanent magnetization m_r in opposite directions. Because of the induced torque, the SMR (voltage over current) will have a slight dependence upon the current. On the right side, we see the effect of the changed remanence on the SMR curve as a function of the effective field (upper panel) and the current density (lower panel). We find a lower SMR value for negative m_r and negative SOT, while SMR is increased for positive m_r and vice versa. This nonlinear second-order effect can be used to detect the positive or negative magnetic state at remanence.

We now evaluate the torque exerted by the spin Hall effect in the Pt/FM bilayers. The coefficient $\Delta\hat{\varrho}_{\mathrm{SMR}}$ as a function of the Pt thickness follows the equation [21]:

$$\Delta\hat{\varrho}_{\mathrm{SMR}} = \theta_{\mathrm{SH}}^2 \frac{1}{x} \frac{\tanh(x)\tanh(x/2)^2}{1 + (G_{Pt}/G_c)\tanh(x)} \tag{3}$$

where $x = d_{Pt}/l_{Pt}$ is the ratio between the thickness and the diffusion length of Pt, θ_{SH} is the spin Hall angle of Pt, $G_{Pt} = \sigma_{e,Pt}/l_{Pt}$ is the effective conductance of Pt, and G_c is the finite conductance at the interface [21]. The fit of the measured data (see Fig. 5) provides $G_c = 1 \cdot 10^{16}\,\Omega^{-1}\mathrm{m}^{-2}$, $\theta_{\mathrm{SH}} = 0.14$, and $l_{Pt} = 1.1 \cdot 10^{-9}$ m. It is therefore possible to

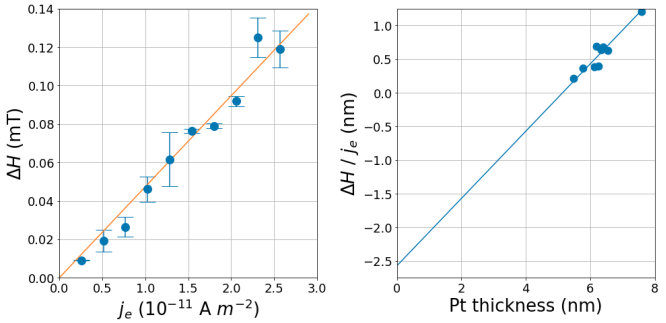

Fig. 6. SMR peaks displacements as a function of the current (left: sample Pt thickness 5.8 nm) and as a function of Pt thickness (right: $I = 10$ mA). Left: linear increase of the SMR peaks shift with the current density is observed. Right: y-axis intercept of the line fit with slope 1/2 delivers, according to (7), the SOT efficiency.

compute the damping-like SOT efficiency [4] as

$$\xi_{\mathrm{DL}} = \theta_{\mathrm{SH}} \frac{\tanh(x)\tanh(x/2)}{1 + (G_{Pt}/G_c)\tanh(x)} \tag{4}$$

which in the range $d_{Pt} = 5$–7 nm turns out to be $\xi_{\mathrm{DL}} = 0.117$.

However, the SOT effective field $\mathbf{H}_{\mathrm{SOT}}$ is subdivided into a field-like and a damping-like part as

$$\mathbf{H}_{\mathrm{SOT}} = H_{\mathrm{DL}}\mathbf{m} \times \hat{\mathbf{z}} + H_{\mathrm{FL}}\hat{\mathbf{z}} \tag{5}$$

where $\mathbf{m}$ is the reduced magnetization of the FM and $\hat{\mathbf{z}}$ is the direction of the moment injected by the spin Hall layer. The two components are given by

$$H_{\mathrm{FL/DL}} = \frac{[(\hbar/2)/e]j_e}{\mu_0\, M_s d_{\mathrm{FM}}} \xi_{\mathrm{FL/DL}} \tag{6}$$

where M_s is the saturation magnetization and ξ_{FL} and ξ_{DL} are the field- and damping-like efficiencies, respectively. The effective field H_{eff} acting on the magnetization becomes the sum of the applied field, the spin–orbit field, and the magnetic field generated by the current j_e, $H_{\mathrm{Oe,z}}$ (the Oersted field). As shown in Fig. 6, the displacement of the SMR curves, applying the field along z, is a function of j_e. The observed field displacement ΔH can be attributed to the effective field, and estimating the spin–orbit field along z by the field-like component only, we obtain $H_{\mathrm{eff,z}} = H_z + H_{\mathrm{FL}} + H_{\mathrm{Oe,z}}$. Therefore, we get the displacement

$$\frac{\Delta H}{j_e} = -\frac{(\hbar/2)/e}{\mu_0\, M_s d_{\mathrm{FM}}} \xi_{\mathrm{FL}} + \frac{d_{Pt}}{2}. \tag{7}$$

From Fig. 6, we can derive $\xi_{\mathrm{FL}} = 0.019$ with the saturation magnetization chosen equal to the effective magnetization obtained from the FMR measurements (see the following) $\mu_0\, M_s = \mu_0\, M_{\mathrm{eff}} = 1.2$ T.

To validate the SOT parameters obtained, we performed independent SOT-FMR measurements followed by an angular-dependent harmonic Hall voltage analysis of the Pt/FeCoB bilayers. First, SOT-FMR was determined for different Pt thicknesses, resulting in the frequency versus in-plane magnetic field relation, modeled using the Kittel formula [22], and the FMR linewidth as a function of frequency—Fig. 7(a) and (b). Thus, the values of the effective magnetization $\mu_0\, M_{\mathrm{eff}} = 1.2$ T was obtained and

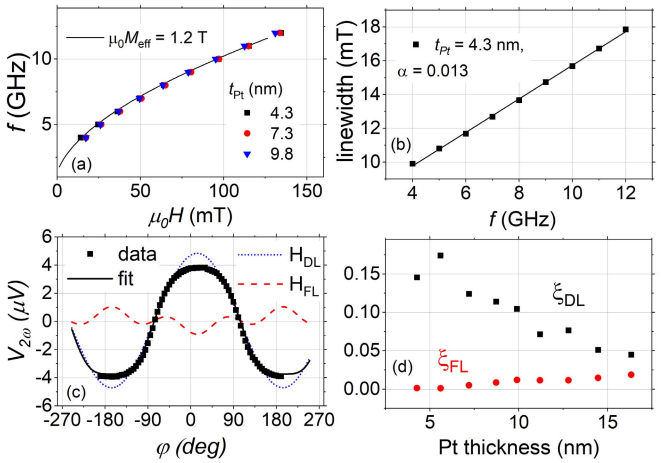

Fig. 7. Spin–orbit torque-induced FMR and harmonic Hall voltage measurements of Pt/FeCoB bilayers. (a) Frequency versus magnetic field dependence modeled using the Kittel formula. (b) Linewidth versus frequency dependence resulting in a magnetization damping coefficient calculation. Example of the angular dependence of the second-harmonic Hall voltage ($V_{2\omega}$) modeled using (8) (c) and the damping- and field-like SOT efficiencies versus Pt thickness.

magnetization damping between $\alpha = 0.013$ and 0.015 depends on the Pt thickness.

Afterward, we determined the SOT components using the analysis of the harmonic Hall signals, based on the approach proposed by Avci *et al.* [23]. To do so, we first measured the resistivity dependence on Pt thickness using the four-point method [3], which decreases from $\rho_{\mathrm{Pt}} = 52 \cdot 10^{-8}$ Ωm for $d_{\mathrm{Pt}} = 4.5$ nm down to $24 \cdot 10^{-8}$ Ω for 14 nm. Then, the first- and second-harmonic Hall signals were determined as a function of the in-plane magnetic field angle (φ_H) for different field magnitudes (H)—Fig. 7(c)—which was than modeled using the formula

$$V_{2\omega} = -A\cos\varphi_H \cos 2\varphi_H - B\cos\varphi_H \tag{8}$$

where $A = (V_P H_{\mathrm{FL}}/H)$ is proportional to the planar Hall voltage V_P and the field-like effective field H_{FL} and $B = ((V_A H_{\mathrm{DL}}/2\ H_{\mathrm{eff}}) - V_{\mathrm{ANE}})$ is proportional to the anomalous Hall voltage V_A and the damping-like effective field H_{DL}. The anomalous Nernst contribution V_{ANE} was found negligible. Modeling the A versus $1/H$ and B versus $1/H_{\mathrm{eff}}$ dependencies with linear functions results in H_{FL} and H_{DL}, which was then converted into the spin–orbit torque efficiency using (6). The dependencies of ξ_{DL} and ξ_{FL} on d_{Pt} are presented in Fig. 7(d). Both SOT efficiencies calculated this way agree well with the values obtained from the SMR measurements in the range $d_{\mathrm{Pt}} = 5$–7 nm.

IV. Conclusion

We performed measurements of SMR in metallic heterostructures consisting of Pt/FeCoB with various Pt thicknesses and magnetocrystalline anisotropy in the film plane. Although the sensing current is not limited to the Pt layer due to the finite resistivity of the FM layer, the resistivity measurement can be almost exclusively ascribed to the SMR effect due to the large difference of the resistances and the AMR and SMR effects. The analysis of the SMR curves

shows a second-order dependence on the sensing current; the spin current generated through the spin Hall effect in the HM causes a torque on the magnetization of the FM layer and changes slightly the magnetization state, which is reflected in the SMR measurement. In the measured Hall bars, the magnetocrystalline anisotropy direction is perpendicular to the current direction, i.e., along the Hall bar. Therefore, the SMR has a low resistance state when the magnetization is aligned with the easy anisotropy axis and a high-resistance state when the magnetization is aligned with the hard anisotropy axis. Due to the fact that the SMR is proportional to the square of the component of the magnetization in the hard direction, any slight change in this component is reflected in the SMR signal. In a structure with a multidomain state, where the magnetization curve has a slope at remanence, this opens up the possibility to sense the magnetization state (positive or negative remanence) by changing from positive to negative current and to perform a magnetization reading. On the other hand, it allows for the determination of the SOT efficiencies by determining the SMR change (damping-like torque; vertical shift of the SMR curve) and the effective SOT field causing a displacement of the SMR curve (field-like torque; horizontal shift).

ACKNOWLEDGMENT

The Project 17FUN08-TOPS has received funding from the EMPIR Programme co-financed by the Participating States and from the European Union's Horizon 2020 Research and Innovation Programme. The work of Witold Skowroński was supported by the National Science Centre, Poland, under Grant UMO-2015/17/D/ST3/00500. The work of Stanisław Łazarski and Krzysztof Grochot was supported by the National Science Centre in Poland under Grant UMO-2016/23/B/ST3/01430 (SPINORBITRONICS).

Microfabrication was performed at the Academic Centre for Materials and Nanotechnology, AGH.

REFERENCES

[1] B. Dieny *et al.*, "Opportunities and challenges for spintronics in the microelectronics industry," *Nature Electron.*, vol. 3, no. 8, pp. 446–459, 2020.

[2] A. Manchon *et al.*, "Current-induced spin-orbit torques in ferromagnetic and antiferromagnetic systems," *Rev. Mod. Phys.*, vol. 91, no. 3, Sep. 2019, Art. no. 035004.

[3] M.-H. Nguyen, D. C. Ralph, and R. A. Buhrman, "Spin torque study of the spin Hall conductivity and spin diffusion length in platinum thin films with varying resistivity," *Phys. Rev. Lett.*, vol. 116, no. 12, Mar. 2016, Art. no. 126601.

[4] C.-F. Pai, Y. Ou, L. H. Vilela-Leão, D. C. Ralph, and R. A. Buhrman, "Dependence of the efficiency of spin Hall torque on the transparency of Pt/ferromagnetic layer interfaces," *Phys. Rev. B, Condens. Matter*, vol. 92, no. 6, Aug. 2015, Art. no. 064426.

[5] L. Liu, T. Moriyama, D. C. Ralph, and R. A. Buhrman, "Spin-torque ferromagnetic resonance induced by the spin Hall effect," *Phys. Rev. Lett.*, vol. 106, no. 3, Jan. 2011, Art. no. 036601.

[6] L. Liu, C.-F. Pai, Y. Li, H. W. Tseng, D. C. Ralph, and R. A. Buhrman, "Spin-torque switching with the giant spin Hall effect of tantalum," *Science*, vol. 336, no. 6081, pp. 555–558, May 2012. [Online]. Available: http://science.sciencemag.org/content/336/6081/555

[7] I. M. Miron *et al.*, "Perpendicular switching of a single ferromagnetic layer induced by in-plane current injection," *Nature*, vol. 476, no. 7359, pp. 189–193, Aug. 2011.

[8] K. Garello *et al.*, "SOT-MRAM 300MM integration for low power and ultrafast embedded memories," in *Proc. IEEE Symp. VLSI Circuits*, Jun. 2018, pp. 81–82.

[9] V. Krizakova, K. Garello, E. Grimaldi, G. S. Kar, and P. Gambardella, "Field-free switching of magnetic tunnel junctions driven by spin–orbit torques at sub-ns timescales," *Appl. Phys. Lett.*, vol. 116, no. 23, Jun. 2020, Art. no. 232406, doi: 10.1063/5.0011433.

[10] D. Zhu and W. Zhao, "Threshold current density for perpendicular magnetization switching through spin-orbit torque," *Phys. Rev. Appl.*, vol. 13, no. 4, Apr. 2020, Art. no. 044078, doi: 10.1103/PhysRevApplied.13.044078.

[11] S. Ingvarsson, G. Xiao, S. S. P. Parkin, W. J. Gallagher, G. Grinstein, and R. H. Koch, "Low-frequency magnetic noise in micron-scale magnetic tunnel junctions," *Phys. Rev. Lett.*, vol. 85, no. 15, pp. 3289–3292, Oct. 2000, doi: 10.1103/PhysRevLett.85.3289.

[12] A. Hirohata *et al.*, "Review on spintronics: Principles and device applications," *J. Magn. Magn. Mater.*, vol. 509, Sep. 2020, Art. no. 166711.

[13] S. Fukami, T. Anekawa, C. Zhang, and H. Ohno, "A spin–orbit torque switching scheme with collinear magnetic easy axis and current configuration," *Nature Nanotechnol.*, vol. 11, no. 7, pp. 621–625, Jul. 2016, doi: 10.1038/nnano.2016.29.

[14] L. Liu, C.-F. Pai, D. C. Ralph, and R. A. Buhrman, "Magnetic oscillations driven by the spin Hall effect in 3-terminal magnetic tunnel junction devices," *Phys. Rev. Lett.*, vol. 109, no. 18, Oct. 2012, Art. no. 186602, doi: 10.1103/PhysRevLett.109.186602.

[15] Y.-T. Liu *et al.*, "Determination of spin-orbit-torque efficiencies in heterostructures with in-plane magnetic anisotropy," *Phys. Rev. Appl.*, vol. 13, no. 4, Apr. 2020, Art. no. 044032.

[16] J. Kim, P. Sheng, S. Takahashi, S. Mitani, and M. Hayashi, "Spin Hall magnetoresistance in metallic bilayers," *Phys. Rev. Lett.*, vol. 116, no. 9, Feb. 2016, Art. no. 097201, doi: 10.1103/PhysRevLett.116.097201.

[17] A. Hubert and R. Schäfer, *Magnetic Domains*. Berlin, Germany: Springer-Verlag, 1998.

[18] M. Althammer *et al.*, "Quantitative study of the spin Hall magnetoresistance in ferromagnetic insulator/normal metal hybrids," *Phys. Rev. B, Condens. Matter*, vol. 87, no. 22, Jun. 2013, Art. no. 224401.

[19] Y.-T. Chen *et al.*, "Theory of spin Hall magnetoresistance," *Phys. Rev. B, Condens. Matter*, vol. 87, no. 14, Apr. 2013, Art. no. 144411. doi: 10.1103/PhysRevB.87.144411.

[20] H. L. Wang, C. H. Du, Y. Pu, R. Adur, P. C. Hammel, and F. Y. Yang, "Scaling of spin Hall angle in 3D, 4D, and 5D metals from $Y_3Fe_5O_{12}$/metal spin pumping," *Phys. Rev. Lett.*, vol. 112, no. 19, May 2014, Art. no. 197201.

[21] J.-G. Choi, J. W. Lee, and B.-G. Park, "Spin Hall magnetoresistance in heavy-metal/metallic-ferromagnet multilayer structures," *Phys. Rev. B, Condens. Matter*, vol. 96, no. 17, Nov. 2017, Art. no. 174412.

[22] C. Kittel, "On the theory of ferromagnetic resonance absorption," *Phys. Rev.*, vol. 73, no. 2, pp. 155–161, Jan. 1948, doi: 10.1103/PhysRev.73.155.

[23] C. O. Avci *et al.*, "Interplay of spin-orbit torque and thermoelectric effects in ferromagnet/normal-metal bilayers," *Phys. Rev. B, Condens. Matter*, vol. 90, no. 22, Dec. 2014, Art. no. 224427, doi: 10.1103/PhysRevB.90.224427.